# Mitigation of energetic ions and keeper erosion in a high-current hollow cathode

IEPC-2015-134／ISTS-2015-b-134

*Presented at Joint Conference of 30th International Symposium on Space Technology and Science*
*34th International Electric Propulsion Conference and 6th Nano-satellite Symposium*
*Hyogo-Kobe, Japan*
*July 4 — 10, 2015*

Benjamin A. Jorns,* Ioannis G. Mikellides,† Dan M. Goebel, ‡ and Alejandro Lopez Ortega §
*Jet Propulsion Laboratory, California Institute of Technology, Pasadena, CA 91109, USA*

**An analytical formulation is presented for the dependence of the energy of ion acoustic turbulence on the steady-state plasma parameters in the near plume of a 100-A $LaB_6$ hollow cathode. This is a critical parameter of interest as it is theoretically and experimentally linked to the energy of erosion-causing ions in the cathode plume. The theoretical formulation for the turbulent energy is experimentally investigated by spatially-resolved measurements along the centerline of the cathode plume. It is shown that in accordance with theoretical expectations, the turbulence grows exponentially downstream of the cathode keeper but that its magnitude also exhibits an exponential decay with flow rate. For flow rates above 8 sccm, a minimum in the turbulent energy with discharge current is observed experimentally. This minimum is shown from first principles to be the result of a balance between electron drift and electron temperature driving the turbulence and ion neutral collisions damping its magnitude. Given the link between ion acoustic turbulence and energetic ions, the ability to predict the minimum in turbulent energy afforded by the validated theoretical formulation is discussed as a promising mechanism for mitigating energetic ions in high current hollow cathodes.**

*Engineer, Electric Propulsion Group, benjamin.a.jorns@jpl.nasa.gov
†Principal Engineer, Electric Propulsion Group
‡Senior Research Scientist, Thermal and Propulsion Engineering Section
§Engineer, Electric Propulsion Group

## Nomenclature

| | | |
|---|---|---|
| $n_s$ | : | Species density |
| $T_s$ | : | Species temperature |
| $m_s$ | : | Species mass |
| $V_s$ | : | Species drift velocity |
| $f_s$ | : | Velocity distribution function of species |
| $E$ | : | Electric field |
| $q$ | : | Fundamental charge |
| $\omega_{ps}$ | : | Species plasma frequency |
| $\nu_{in}$ | : | Ion-neutral collision frequency |
| $\phi_k$ | : | Potential amplitude of acoustic mode with wavenumber $k$ |
| $\omega$ | : | Wave frequency |
| $\vec{k}$ | : | Wave vector |
| $c_s$ | : | Ion acoustic speed |
| $\lambda_{de}$ | : | Debye length |
| $\epsilon$ | : | Dielectric tensor of plasma |
| $W_k$ | : | Wave energy density for mode with wavenumber k |
| $N_k$ | : | Wave action for mode with wavenumber k |
| $E_T$ | : | Total wave energy |
| $\dot{m}$ | : | Flow rate |
| $I_D$ | : | Discharge current |
| $\phi_0$ | : | Plasma potential |
| $r_0$ | : | Keeper orifice radius |

## I. Introduction

Keeper erosion represents one of the major failure modes for hollow cathodes. Previous endurance tests have shown that the discharge cathode of an ion engine will erode after 30,000 hrs,[1,2] while under extreme circumstances such as high current operation, keeper failure can occur in less than 8,000 hrs.[3] This lifetime is inadequate for the next generation of deep space missions that call for high power (> 50 kW), long-duration (50,000 hrs) systems. Understanding and ultimately mitigating keeper erosion is therefore of paramount importance for the future development of high power electric thrusters.

While keeper erosion has been linked to the sputtering that results from the impact of high energy ions originating from the cathode plume, it is not known why and how these energetic ions form. Classical processes such as electrostatic acceleration are too small to explain the observed energies, and to date, there has not been a consensus reached as to what non-classical mechanism could drive the ion formation. For example, while work by Goebel et al.[4] and Mikellides et al.[5] showed that the erosion at one operating point of the NSTAR discharge cathode can be attributed to the onset of large amplitude ($\sim$ 100% background), low-frequency potential oscillations in the plume, there are other operating points for this cathode where the low-frequency oscillations are low (< 1% background) and yet high energy ions persist. Studies on other hollow cathodes have supported these findings: high energy ions will appear even when the oscillation levels in the plume are small.[6,7] It thus would seem that while under some circumstances we can explain the energetic ions, there are still many cases where the driving mechanisms remain unknown.

We have worked to understand these outstanding anomalous processes through a two year internal research program at the NASA Jet Propulsion Laboratory. Our initial investigation resulted in the experimental detection of ion acoustic turbulence (IAT) in the plume of a 100-A class $LaB_6$ cathode.[8] This in turn confirmed the theoretical arguments made previously by Mikellides et al[5,9] that non-classical resistivity due to two-stream instabilities must persist in the near plume of these devices. In a follow on investigation, we postulated that in addition to being the source of non-classical resistivity, the ion acoustic turbulence may also drive the formation of energetic ions through collisionless Landau damping.[10] To support this conjecture, we first demonstrated a correlation between ion acoustic turbulence and the formation of energetic ions in the 100-A cathode, and then, through a one-dimensional, quasilinear model, we showed that the amplitude of the acoustic turbulence was sufficient to explain the high ion energies that appeared at high discharge currents. We also noted in this work that the collisionless energy exchange between the turbulence and ions should be characterized by a formation of a high energy tail, which is consistent with the experimental observations of non-thermalized tails in other high current cathodes.[6]

To date, our work has served to show a correlational and causal link between the formation of ion acoustic turbulence and the onset of energetic ions in a high current cathode. This suggests that minimizing the turbulence will reduce the energetic ions, thereby leading to a low erosion state. The purpose of this investigation is to exploit this fact by demonstrating a mitigation technique that is most easily realized from an operations perspective: identifying an operating point, for a desired discharge current, that results in low levels of turbulence. To this end, we begin in the first section by showing from first principles that the total wave energy of the turbulence should scale with the ion energy. In the second section, we present a theoretical formulation for how the wave energy depends on cathode plasma parameters. In the third and fourth sections, we experimentally measure the correlation between wave and ion energy and then attempt to validate our analytical results with these measurements. In the final section, we discuss our results in the context of developing guidelines for minimizing turbulence (and consequently energetic ions) in high current hollow cathodes.

## II. Theory

### A. Ion acoustic turbulence

The ion acoustic wave is an electrostatic mode that frequently occurs in plasmas with a large disparity in ion and electron temperatures: $T_e \gg T_i$. It propagates in the ion frame of reference with the ion sound speed, and it can be driven unstable by the inverse Landau damping that occurs when the electron drift exceeds the wave phase velocity. In this case, the wave gains energy at the expense of electron momentum.

For an unmagnetized, collisionless plasma with $T_e \gg T_i$, plasma parameter gradient lengthscales longer than the characteristic wavelength of the modes $k^{-1} \ll L$, and $\omega \ll \omega_{pi}$, the dispersion relation for the ion acoustic wave can be written as

$$D\left(\vec{k},\omega\right) = \vec{k}\cdot\varepsilon\cdot\vec{k} = k^2 - \omega_{pi}^2\left[-\frac{m_i}{T_e} + \frac{k^2}{(\omega')^2}\right] - i\left[\left(\frac{\pi}{2}\right)^{1/2}\left(\frac{\vec{k}\cdot\left(\vec{V}_e - \vec{V}_i\right) - \omega'}{k\lambda_{de}^2 v_e}\right)\right] \tag{1}$$

$$-\left[\omega_{pi}^2\left(\frac{\pi}{2}\right)^{1/2}\left(\frac{m_i}{T_i}\right)^{3/2}\frac{\omega'}{k}e^{-m_i\left(\omega'/k\right)^2/(2T_i)}\right], \tag{2}$$

where $\omega' = \omega - \vec{k}\cdot\vec{V}_i$ is the frequency in the ion frame of reference. Solving the real component of the dispersion relation yields the dependence of frequency on wavenumber

$$\omega = \left(c_s k + \vec{k}\cdot\vec{V}_i\right), \tag{3}$$

where $c_s = \sqrt{T_e/m_i}$ is the ion acoustic speed. This dispersion relation indicates that the acoustic mode propagates in the laboratory frame at a speed equal to the sum of the ion drift and ion acoustic velocities. We have verified this dispersion experimentally for the cathode plume subject to our investigation.[8]

We can use Eq. 3 coupled with the imaginary component of the dielectric response in Eq. 2 to find the imaginary component of the frequency, i.e. the growth rate:

$$\gamma_k = \omega'\left(\frac{\pi}{2}\right)^{1/2}\left[\left(\frac{\vec{k}\cdot\left(\vec{V}_e - \vec{V}_i\right) - c_s k}{k v_e}\right) - \left(\frac{T_e}{T_i}\right)^{3/2} e^{-\frac{T_e}{2T_i}}\right]. \tag{4}$$

The first term on the right hand side represents the contribution from inverse Landau damping on the electrons. As the relative drift between electrons and ions increases, this contribution becomes larger. The second term includes the effects of ion Landau damping. Typically in the cathode plume, the phase velocity of the wave significantly exceeds the ion thermal velocity such that $T_e \gg T_i$. This allows us to neglect the ion Landau damping term in comparison to the electron contribution:

$$\gamma_k = \omega' \left(\frac{\pi}{2}\right)^{1/2} \left(\frac{\vec{k} \cdot \left(\vec{V}_e - \vec{V}_i\right) - c_s k}{k v_e}\right). \tag{5}$$

Finally, we note from Eq. 5 that the growth is maximized when the $\vec{k} \| \left(\vec{V}_e - \vec{V}_i\right)$ such that we anticipate the dominant mode to be in this direction. This is consistent with what has been found in previous theoretical and experimental investigations (c.f. Ref. 11). We therefore constrain $\vec{k}$ to this direction for the remainder of this investigation, and the final expression for the growth rate becomes

$$\gamma_k = \omega' \left(\frac{\pi}{2}\right)^{1/2} \left(\frac{V_e'}{v_e}\right), \tag{6}$$

where we have defined $V_e' = \left|\vec{V}_e - \vec{V}_i\right|$ and made the physically reasonable approximation that the relative electron-ion drift exceeds the ion sound speed $V_e' \gg c_s$. In a plasma characterized by strong electron drift such as the cathode plume, we thus see that the wave grows at the expense of electron momentum. The slowing down of the electrons that results from this process can be represented as an effective resistivity, which as we showed in Ref. 8, can be dominant over classical effects.

It is at this point we note that the effects of classical collisions have not been incorporated into this formulation. While we do not anticipate electron collisions to play a large role since the wave is primarily carried by ions, ion-neutral collisions with frequency $\nu_{in}$ can and do damp waves below a cutoff frequency. To first order this effect be included by subtracting $\nu_{in}$ from Eq. 6. However, since the ion acoustic wave can propagate with frequencies up to $\omega = \omega_{pi}$, we anticipate that when we formulate the growth of the turbulent spectrum (which is spread out over $\omega$), the effect of this low frequency damping term on the linear growth of the total wave energy will be small.

### B. Relationship between ion energy and turbulence energy

In our previous theoretical and experimental investigation of IAT in hollow cathode plumes,[10] we found both a causal and correlational relation between the onset of turbulence and the formation of energetic ions. We employed a one-dimensional model for the collisionless interaction of the turbulence with an ion distribution function, and we showed that acoustic turbulence led to the formation of a high energy tail. The purpose of this section is to approximate this inherently kinetic effect with macroscopic parameters, i.e. to find a simple scaling relation between the energy of the turbulence and the average energy in the ion distribution function. The advantage of this approach is that it permits a direct comparison between ion energy and wave energy over a wide range of operating conditions. It also provides us with the governing parameter that we should seek to minimize in order to identify an operating point with the lowest levels of energetic ions. With this in mind, we first introduce a kinetic formulation for the ion velocity distribution and then average over velocity space to find the macroscopic quantities.

The interaction of the ion velocity distribution function in the direction of wave propagation ($\vec{v} \| \vec{k}$) can be modeled by a Boltzmann equation:[12]

$$\frac{\partial f_i}{\partial t} + v\frac{\partial f_i}{\partial x} + \frac{q}{m_i}E\frac{\partial f_i}{\partial v} = \frac{\partial}{\partial v}\left[D_{QL}\frac{\partial f_i}{\partial v}\right], \tag{7}$$

where we have denoted the direction of propagation as $x$, neglected classical collisions and ionization, and represented the interaction of the turbulence with the ion distribution as a quasilinear diffusion operator, $D_{QL}$. The quasilinear model for the interaction of the turbulence with the ion distribution function is predicated on the assumption of low level turbulence compared to the electron thermal energy in the plasma and the random phase approximation.[13] The first assumption is supported by our previous experimental observations of turbulence in the plume and the second is satisfied by the fact that the acoustic modes are turbulent, i.e. with random phase.

With this in mind, we can write the diffusion operator as[14]

$$D_{QL} = \frac{q^2}{m_i^2}\sum_k \left[k\phi_k\right]^2 \pi\delta\left(\omega - kv\right) - \gamma_k \frac{\partial}{\partial\omega}\mathcal{P}\left[\frac{1}{\omega - kv}\right], \tag{8}$$

where $\mathcal{P}$ denotes the principal value. Eqs. 7 and 8 model the effective spreading in the ion distribution function that results from the ion interaction with the acoustic turbulence. Part of this effect is attributed to ion Landau damping, which is captured by the first term in Eq. 8. This represents the net energy exchange with the waves that occurs when ions are stationary in the wave frame of reference, $v = \omega/k$. The second term represents the fact that the ion acoustic wave is carried by the ions themselves. There is an energy associated with the propagation of the wave, i.e. the sloshing back and forth of the ions as the mode is carried through the plasma. For a single wave with a fixed frequency and wavenumber, this wave energy translates to a periodic variation in the ion velocity distribution function at frequency $\omega$. However, since the ion acoustic waves are turbulent with random phase, all of these periodic oscillations deconstructively interfere and the energy associated with the turbulent propagation can lead to a net broadening in the ion velocity distribution function. This non-resonant effect is captured by the second term in Eq. 8.

In Ref. 8, we solved Eq. 7 for the plasma parameters and turbulent amplitudes experimentally measured in a 100-A $LaB_6$ cathode. However, in the interest of collapsing this effect into a macroscopic parameters, we take the zeroth and first moments:

$$\frac{\partial n_i}{\partial t} + \frac{\partial \left[n_i V_i\right]}{\partial x} = 0 \tag{9}$$

$$\partial_t \left[n_i V_i\right] + \partial_x \left[n_i \langle v\rangle^2\right] - \frac{q n_i}{m_i} E = -\int \left[D_{QL} \frac{\partial f_i}{\partial v}\right] dv, \tag{10}$$

where $\langle ..\rangle$ denotes the average over velocity space. We now assume that the cathode plume has evolved to a stationary condition such that we can neglect the time-dependent term:

$$\partial_x \left[n_i \langle v^2\rangle\right] + \frac{q n_i}{m_i} \partial_x \phi_0 = -\int \left[D_{QL} \frac{\partial f_i}{\partial v}\right] dv, \tag{11}$$

where we have represented the electric field as the gradient of the steady-state plasma potential $E = -\partial_x \phi_0$. Invoking the identify $\langle v^2\rangle = \sigma^2(v) + V_i^2$ where $\sigma$ denotes the variance, we rewrite Eq. 11 as

$$\partial_x \left[n_i \left(\sigma^2(v) + V_i^2\right)\right] + \frac{q n_i}{m_i} \phi_0 = -\int \left[D_{QL} \frac{\partial f_i}{\partial v}\right] dv. \tag{12}$$

Finally, we employ the first equation from Eq. 10 to further simplify this expression to

$$-m_i \int \left[D_{QL} \frac{\partial f_i}{\partial v}\right] dv = \partial_x \left[n_i m_i \sigma^2(v)\right] + n_i \partial_x \left[\frac{1}{2} m_i V_i^2\right] + q n_i \partial_x \phi_0. \tag{13}$$

For ion acoustic turbulence, we can show (see Appendix) that the left hand side of Eq. 13 can be written as

$$-m_i \int \left[D_{QL} \frac{\partial f_i}{\partial v}\right] dv = \frac{\partial}{\partial x} W_T + \frac{1}{c_s} P_T \zeta, \tag{14}$$

where $W_T = \sum_k W_k$ is the total wave energy density of the acoustic turbulence, $P_T = \sum_k \omega(k) W_k$ is the total power flux of the acoustic turbulence, and

$$\zeta = \left[\left(\frac{\pi}{2}\right)^{1/2} \left(\frac{T_e}{T_i}\right)^{3/2} e^{-T_e/2T_i}\right]. \tag{15}$$

The terms in Eq. 14 lend themselves to an intuitive physical description. The first encapsulates the aforementioned non-resonant effects and represents the total kinetic energy associated with the propagation of the wave. The second represents the introduction of energy into the ion distribution function through collisionless damping. The factor $\zeta$ takes into account that only a fraction of the ion population satisfies the resonant condition ($v = \omega/k$) and therefore is susceptible to this collisionless energy exchange.

Both resonant and non-resonant effects in Eq. 14 contribute to the increase in the total ion energy, and as we showed in Ref. 8, they work in concert to generate a high energy tail. However, since the cathode plasma is characterized by $T_e/T_i \gg 1$ such that $\zeta \to 0$, we can see that the primary contribution to the ion energy from the ion acoustic turbulence stems from the non-resonant term. We therefore approximate Eq. 14 as

$$\partial_x \left[n_i m_i \sigma^2\left[(v)\right]\right] + n_i \partial_x \left[\frac{1}{2} m_i V_i^2\right] + q n_i \partial_x \phi_0 = \frac{\partial}{\partial x} W_T. \tag{16}$$

Finally, we invoke the definition of electrostatic wave energy density to find

$$W_T = \frac{\epsilon_0}{2} \sum_k \omega \left[k\phi_k\right]^2 \frac{\partial \epsilon}{\partial \omega} = n_i \sum_k \frac{\left[q\phi_k\right]^2}{T_e} = n_i E_T, \tag{17}$$

where we have defined the total energy in the spectrum as $E_T = \sum_k \left[q\phi_k\right]^2 / T_e$. This simplification in turn allows us to write

$$\partial_x \left[n_i m_i \sigma^2 \left(v\right)\right] + n_i \partial_x \left[\frac{1}{2} m_i V_i^2\right] + q n_i \partial_x \phi_0 = \partial_x \left[n_i E_T\right]. \tag{18}$$

To reduce this expression further, we note that we are interested in the energy of ions impacting the cathode keeper, an element that typically floats close to facility ground. The technique we use to measure the ion energies similarly is referenced with respect to ground (Sec. III.B). Since the drift velocity for ions born in the plume is expected to be relatively small,[15] we anticipate that their translational energy at the keeper will be dominated by the electrostatic acceleration from the potential drop from the plume to ground, $\phi_0$. This allow us to identify $\partial_x \left[1/2 m_i V_i^2 + \phi_0\right] = 0$, which coupled with Eq. 14 yields

$$m_i \sigma^2 \left(v\right) = E_T. \tag{19}$$

This expression reflects the physically intuitive result that the total energy of the turbulence stems from the sloshing of ions around the mean velocity, i.e. the spread in the ion energy distribution around the bulk velocity. As mentioned above, it does not account for energy introduced from resonant coupling, so the correlation is not entirely correct. However, in a sense this expression does capture the possibility of high energy tail formation since such an effect increases with wave amplitude and does lead to a net spreading of the ion energy distribution. Armed with Eq. 19, we now can confine our theoretical discussion to one metric about the turbulence, the total local energy. Indeed, if we can understand the dependence of this term on plasma parameters, we should be able to infer the conditions for the formation of energetic ions. We present a theoretical formulation for this term in the next section.

### C. Dependence of turbulence energy on plasma parameters

With the assumption of low amplitude oscillations compared to the plasma thermal energy, the spatial evolution of waves in the cathode plasma is given by the plasma wave kinetic equation (c.f. Chap. 4 of Ref. 14):

$$\frac{\partial N_k}{\partial t} + \frac{\partial \omega}{\partial k} \frac{\partial N_k}{\partial x} - \frac{\partial \omega}{\partial r} \frac{\partial N_k}{\partial k} = 2\gamma_k N_k, \tag{20}$$

where $N_k = W_k/\omega$ is the wave action. This relation is an analog for the density conservation of each species in the plasma, where the wave action is the density of wave packets with wavenumber $k$. While this quantity is conserved if there is no growth rate, the inverse Landau damping from the electrons in the plume provides a source term. For the case of ion acoustic waves we have $\omega = \left(c_s + V_i\right) k$, and as is consistent with experimental observations,[10] we assume that along cathode centerline, the electron temperature and ion drift are approximately constant. Subject to these assumptions, we take the first moment of Eq. 20 with respect to $\omega$ to find an evolution equation for the total wave energy density

$$\left(c_s + V_i\right) \frac{\partial W_T}{\partial x} = \sqrt{2\pi} \left(\frac{V_e'}{v_e}\right) \int \omega W_k d\omega, \tag{21}$$

where we have $W_T \int \omega N_k d\omega$, we have substituted for the group velocity $\partial\omega/\partial k$, and we have used the acoustic growth rate, $\gamma_k$.

Evaluating the integral in Eq. 21 poses a problem since we do not know a priori the frequency dependence of $W_k$. We can resolve this difficulty in part by looking to previous theoretical treatments of acoustic turbulence. These works suggest that non-linear terms in Eq. 20 that we have neglected in our linear formulation will lead to a re-distribution of energy in frequency space.[11,16] The result is a cascade in $\omega$, which as we showed in Ref. 8 for our high current cathode leads at high frequency to a form for $W_k$ as

$$W_k = A\omega^{-\alpha}, \tag{22}$$

where $A$ and $\alpha$ are constants with $\alpha > 2$. It is important to note that while this spectrum is unbounded as $\omega \to 0$, we anticipate that at low frequency, either collisions or length scale considerations will cut off the spectrum. Indeed, if the characteristic gradient length scales in the background plasma $L$ are two short compared to the wavelength $L < 2\pi/k$, the acoustic mode will not propagate. We therefore define an effective cut off wavenumber $k_c = 2\pi/L$ with associated cutoff frequency $\nu_c = (c_s + V_i)\, k_c$ where we have $W_k = 0$ for $\omega < \nu_c$. With this functional form for the distribution of wave energy density, we can perform the integral in Eq. 21 to find

$$(c_s + V_i)\,\frac{\partial W_T}{\partial x} = \beta\nu_c\left(\frac{V_e'}{v_e}\right)W_T, \tag{23}$$

where we have defined $\beta = \sqrt{2\pi}\,(\alpha - 1)\,/\,(\alpha - 2)$. We now can integrate this condition from an initial point at the keeper face $x = 0$ to a distance $x$ downstream. This yields the evolution of the total wave energy density

$$W_T = W_0 \exp\left[\frac{\beta\nu_c}{c_s + V_i}\left(\frac{V_e'}{v_e}\right)x\right], \tag{24}$$

where we have defined the initial energy density of the waves as $W_0$.

Determining the form of the initial energy density requires an understanding of the spontaneous thermal fluctuations that seed the acoustic turbulent distribution. We reason that the energy in these initial fluctuations should represent a balance between the thermal energy in the plasma and wave damping effects, namely ion-neutral collisions. To this end, we assume an initial form $W_0 = A' n_i T_e \exp\left[-\eta\nu_{in}'\right]$ where $\eta$ and $A'$ are constants. This is physically the equivalent of setting the initial conditions of the wave propagation to a point upstream of the keeper exit $x = d < 0$ where the plasma is highly collisional with ion-neutral frequency $\nu_{in}'$ and there is little ion drift velocity $V_i \approx 0$. The turbulence is actively damped in this case with $\gamma_k \sim -\nu_{in}'$ and as the spectra propagates downstream toward the keeper, we anticipate this initial wave energy density will decrease as $W_T \propto A' T_e \exp[-d\nu_{in}'/c_s]$. At the keeper exit, the neutral collisions become negligible compared to the electron driven growth and the wave dynamics are governed by Eq. 23 with growth rate given by Eq. 6. The initial energy density at $x = 0$, the keeper exit, is the energy density of the turbulence emerging from the collisional regime: $A' T_e \exp[-d\frac{\nu_{in}}{c_s}]$ where $d$ is the length scale of the distance from the region of high collisionality, e.g. the cathode end cap, to the keeper ($\sim 5$ mm). Using this result as the form of $W_0$, Eq. 21 becomes

$$W_T = n_i A' T_e \exp\left[\left(\frac{\beta\nu_c}{c_s + V_i}\left(\frac{V_e'}{v_e}\right)x - d\frac{\nu_{in}}{c_s}\right)\right]. \tag{25}$$

We divide this result by density to find

$$E_T = A' T_e \exp\left[\left(\frac{\beta\nu_c}{c_s + V_i}\left(\frac{V_e'}{v_e}\right)x - d\frac{\nu_{in}}{c_s}\right)\right]. \tag{26}$$

This result indicates that the total turbulent energy will increase exponentially with distance from the keeper. The growth in turn is modified by the ion-neutral collision frequency, where we can see the collisions act to reduce the total energy in the spectrum. At higher flow rates—and by extension higher ion-neutral collision frequency—the energy in the turbulence will fall exponentially. With Eq. 26, we are now in a position to determine how the background plasma parameters impact wave growth. This is significant in light of Eq. 19, as we anticipate the turbulence to govern the onset of energetic ions. In the next section we describe our experimental investigation to examine the validity of both Eqs. 19 and Eq. 26.

## III. Experimental Setup

### A. Cathode Assembly

We show in Fig. 1 the 100-A cathode assembly[17] we employed for this experimental investigation. This setup consists of a graphite tube that houses a $LaB_6$ insert. A tantalum coaxial heater surrounds this tube, and the assembly is capped with a tungsten endplate with a 3 mm radius orifice. This assembly is then enclosed in a graphite keeper with a 1.5 cm radius and a 0.5 cm radius orifice. The cathode was installed in a 2.8 m

× 1.3 m cylindrical chamber with vacuum maintained by two cryopumps. The base pressure of this facility was $\sim 10^{-7}$ T while at the maximum flow rate we examine here, 15 sccm xenon, the background pressure was maintained at $4 \times 10^{-4}$ T. A water-cooled, copper cylinder that was lined with tungsten served as the anode. This was placed $\sim 3$ cm downstream of the keeper face. While the cathode setup was surrounded by a solenoid capable of generating a magnetic field, for the measurements reported here, no magnetic field was applied.

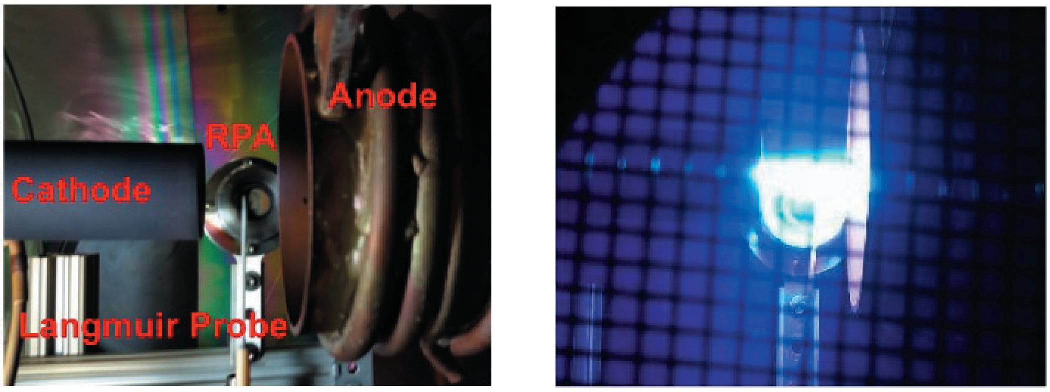


(a) (b)

Figure 1: a) 100-A hollow cathode setup employed in the experiment. The retarding potential analyzer and Langmuir probe are indicated. b) Photograph of cathode in operation at 100 A and 10 sccm.

### B. Diagnostics

We employed a translating Langmuir probe and a stationary retarding potential analyzer to examine plasma and wave properties in the hollow cathode plume. We outline in the following section these diagnostics and our analysis techniques for the data from these probes.

#### *1. Langmuir Probe*

We implemented a translating, cylindrical Langmuir probe to measure the background plasma density, electron temperature, and plasma potential along cathode centerline. The exposed element of the Langmuir probe was tungsten, 1.5 mm in length with a diameter of 0.5 mm, and the probe was capable of translating from 3-30 mm downstream of the cathode keeper. Electron temperature measurements were generated by sweeping the voltage on the probe and recording the resulting current. We then applied an exponential fit to the probe IV trace to find $T_e$ (c.f. Ref. 18), and we invoked the thin sheath approximation for cylindrical probes to estimate density, $n_i = i_{sat}/\left(0.61 q A_p \sqrt{T_e/m_i}\right)$ where $A_p$ denotes the probe area and $i_{sat}$ is the ion saturation current. We estimated the local plasma potential by employing the knee technique. The measurements reported here were generated from an average of thirty-two probe traces.

#### *2. Retarding Potential Analyzer*

In order to characterize ion energy, we employed a four-grid, retarding potential analyzer (RPA). The first grid of the RPA was allowed to float; the second, electron-repelling grid was biased negatively with respect to ground; the third grid provided the bias voltage necessary to resolve ion energies; and the fourth grid was negatively biased to suppress secondary electrons. The collector plate was grounded through a 1 MHz resistor, and we inferred the ion current from the drop across this element. We generated IV characteristics for this setup by incrementing the RPA bias with a DC power supply at 1 V intervals from 0 to 80 V and measuring the time-averaged current at each voltage. Each scan lasted approximately two minutes.

The IV characteristics from the RPA yield information on the distribution of ion-to-charge energies in the plasma. Without *a priori* knowledge of the fraction of multiply charged states in the plasma, the interpretation of the IV characteristic is problematic. However, provided the plasma is dominated by singly charge species, this diagnostic serves as a proxy for ion energy[19]

$$-\frac{dI}{d\varphi} \approx Cq^2 f_i\left(q\varphi\right), \tag{27}$$

where $C$ is a constant, $q$ denotes the elementary charge, $\varphi$ is the probe bias, and $f_i$ is the ion energy distribution function. Due to the limited space between the keeper and the anode, it was necessary to place the RPA at a distance of 7 cm from the cathode centerline (compared to a plume diameter of $\sim 2$ cm) with its grids parallel to the plane containing the centerline. As such, the RPA was only capable of measuring ion energy in the radial direction.

#### 3. *Ion saturation probe*

Electrostatic modes such as the ion acoustic wave are characterized by $\phi \approx (T_e/q)\,\tilde{n}_i/\bar{n}_i$, where $\tilde{n}_i$ is the fluctuating density and $\bar{n}_i$ is the time-averaged density. We can use this relationship to estimate the wave potential amplitude provided we can measure the fractional fluctuations in ion density. To this end, we biased the Langmuir probe outlined in Sec. 1 to -30 V and monitored both the fluctuating and time-averaged components of the ion saturation current. Since $i_{sat} \propto n_i$, we found (under the assumption of constant $T_e$)

$$\phi = \frac{T_e}{q}\frac{\tilde{i}_{sat}}{\bar{i}_{sat}}. \tag{28}$$

The ion saturation probe is simple to implement, and in light of Eq. 28, it is reliable for estimating fluctuation intensity provided $\tilde{i}_{sat} \ll \bar{i}_{sat}$. For this investigation, we primarily were interested in the frequency dependence of the turbulent energy. We therefore report the power spectrum of the potential oscillations divided by the electron temperature (Eq. 17), as a function of position in the cathode plume. In all cases, the power spectra shown are the averaged from 50 time periods and have a resolution of 10 kHz.

## IV. Results

We present in the following section the results from our experimental investigation of the wave and ion energy in the cathode plume. We begin with a discussion of the background plasma parameters and how they approximately satisfy the assumptions governing the linear theory outlined in Sec. II. We then present results for spatial wave growth in the plume and examine the impact of operating conditions on wave energy. We conclude with a comparison between our theoretical predictions for wave and ion energy. The data reported here represents five flow conditions, 5, 8, 10, 12, and 15 sccm, over a range of discharge currents from 7.5 A to 170 A. There is an upper bound on the discharge current investigated for the lower flow rates, as we found that attempting to draw high current at these conditions would cause feedback problems in the cathode power supply.

### A. Background plasma parameters

We show in Fig. 2(a) the plasma density as a function of distance from the keeper for the flow rate of $\dot{m} = 15$ sccm. In all cases the plasma density exhibits an inverse dependence on distance from the cathode with a characteristic length scale $L = n_e/\nabla n_e$ of $3-4$ cm. We have found this value to be constant over the range of operating parameters we investigated. For ion acoustic waves with an electron temperature of $T_e \approx 3$ eV, this length scale corresponds to a cutoff frequency (Sec. III.C) of $\nu_c = 40 \sim 80$ kHz. We do not anticipate waves to propagate below this frequency. For modes with frequencies above this value, however, the wavelengths are sufficiently short that the constant density approximation in Sec. II is approximately satisfied. We estimate this constant density value by taking the spatial average, which we show in Fig. 2(b), as a function of discharge current for the flow rate conditions investigated. The resulting plots indicate that with the exception of the high current values for the $\dot{m} = 12$ sccm case, the density increases linearly with discharge current and is practically independent of flow rate.

We show in Fig. 3(a) the electron temperature as a function of axial position for fixed discharge current, $I_D = 20$ A, and increasing flow rate. Fig. 3(b) depicts the temperature as a function of axial position from keeper for fixed flow rate, $\dot{m} = 15$ sccm, and increasing discharge current. Over the experimental range of interest, we can see that the electron temperature is approximately constant with just a slight increase

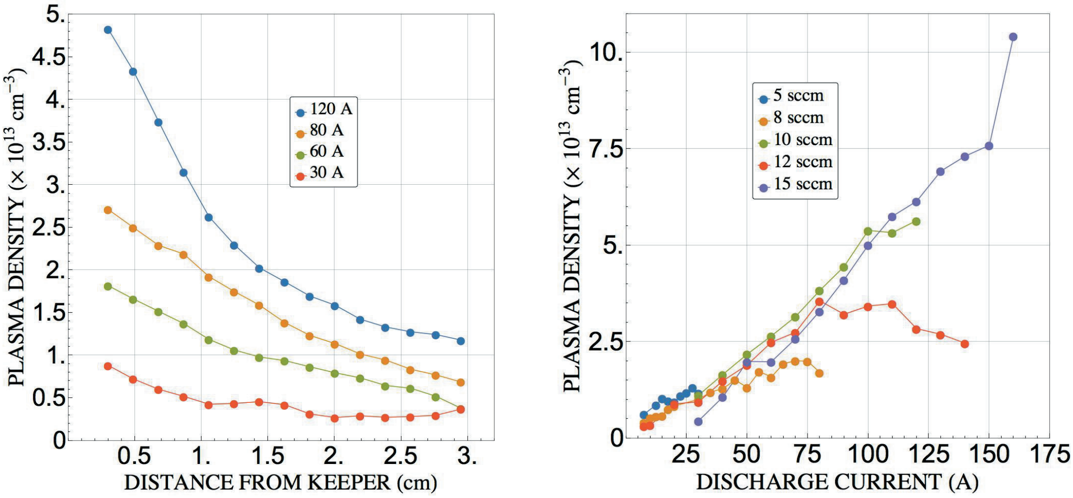


(a) (b)

Figure 2: a) Plasma density as a function of distance from keeper face on cathode line. The flow rate is 15 sccm. b) The spatially averaged plasma density as a function of discharge current for the five investigated flow rates. The error for all the cases shown is ±50%

downstream. This observation supports the assumption made in Sec. II of constant electron temperature along cathode centerline, and as such, we show in Fig. 4(a) the spatially averaged electron temperature over all the flow conditions as a function of discharge current. This plot illustrates how the electron temperature increases almost linearly with discharge current and how the slope of this relationship decreases with flow rate. We also have found that the plasma potential along centerline is constant in our experimental domain, and we show in Fig. 4(b) the spatially-averaged value of this potential as a function of discharge current. This plot illustrates how the potential generally decreases and then asymptotes with discharge current.

In sum, the results of our background plasma measurements give us increased confidence that the homoge-

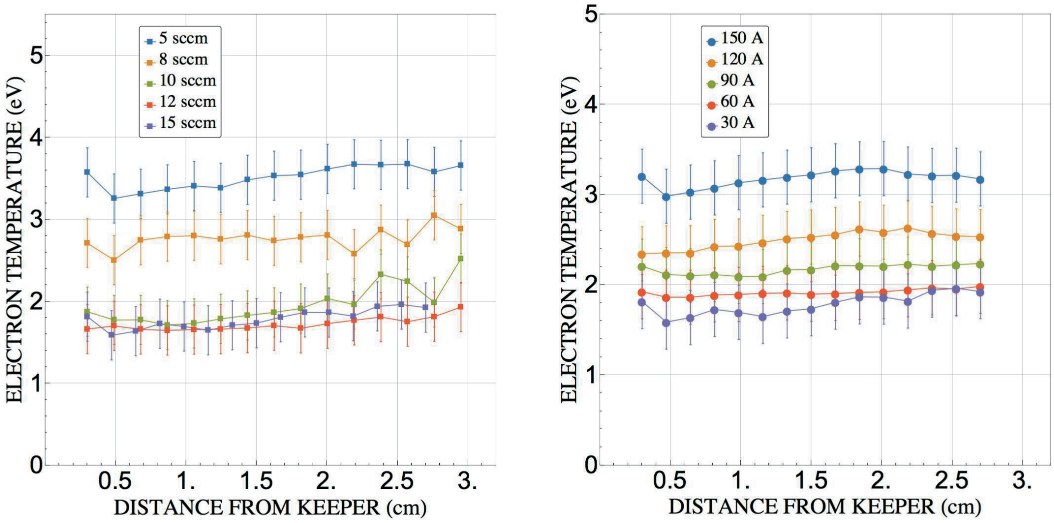


(a) (b)

Figure 3: a) Electron temperature as a function of distance from the keeper for fixed discharge current, $I_D = 20$ A and increasing flow rate. b) Electron temperature as a function of distance from the keeper for fixed flow rate, 15 sccm current, and increasing discharge current.

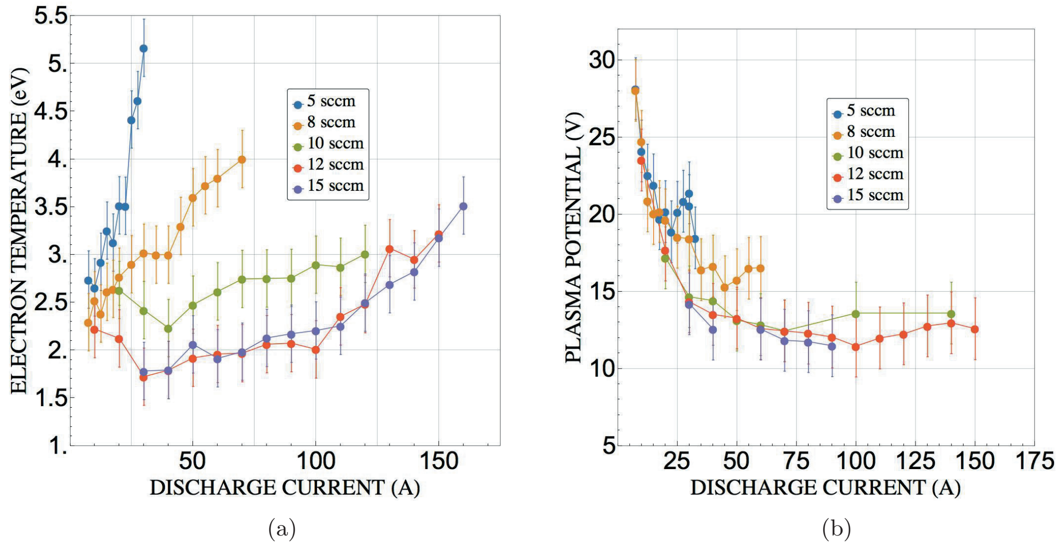


Figure 4: a) Spatially averaged electron temperature as a function of discharge current for all flow rates investigated. b) Spatially averaged plasma potential as a function of discharge current for all flow rates investigated.

nous plasma assumptions we outlined in Sec. II are approximately satisfied on centerline. This facilitates the comparison between our theoretical formulation and experimental results that we explore in the following sections.

### B. Wave Properties

In Ref. 10 we demonstrated with dispersion measurements in the cathode plume that ion acoustic modes propagate in the plasma and that they are characterized by a power spectrum that obeys an inverse dependence on frequency. Since we have established this property of the IAT, in lieu of performing dispersion relation measurements at each operating condition, we instead take a frequency decay commensurate with Eq. 22 as indicative of the presence of the IAT. This permits us to perform spatially resolved single-point measurements of the fluctuations and still infer the presence of the turbulence. For example, we show in Fig. 5(a) the spectrum of the wave energy $\phi^2(\omega)/T_e$ in the cathode plume as a function of axial position for the case of 10 sccm at 100 A discharge. It is immediately evident from this plot that the spectra exhibit the characteristic fall off with frequency outlined in Eq. 22. We note too that the spectra decay precipitously below $\sim 100$ kHz. This cutoff value is comparable to the range we calculated based off the density gradient in Sec. A, and it appears that it is the combination of this cutoff coupled with the inverse cascade that gives rise to the maximum in frequency space exhibited by the spectra. We also see from this data that the turbulence grows in the downstream direction. This is consistent with our interpretation of the turbulence being driven unstable by the plasma as it convects.

We show in Fig. 5(b) the energy spectra as a function of position for $\dot{m} = 5$ sccm and a discharge current of $I_D = 20$ A. In contrast to the results from Fig. 5(a), these plots clearly show two maxima in frequency space. The higher frequency peak corresponds to the ion acoustic instability and exhibits the same trends we discussed for Fig. 5(a). The lower peak is a mode we identified in previous work with an ionization-type instability[8]— much like the oscillation Goebel et al.[4] attributed to the creation of high energy ions in the NSTAR cathode. The mechanism for this type of instability to introduce energy to the waves depends on the fluctuation levels being much larger than the background plasma potential. This is not the case here as the turbulent amplitude is clearly $\ll T_e$, and it is for this reason that we largely dismissed these waves in Ref. 8 as a contributor to the onset of energetic ions in the 100-A cathode. We therefore are only interested in this investigation in the ion acoustic modes, and we control for the presence of the second low-frequency mode by only integrating over the portion of the frequency spectrum where the ion acoustic spectrum clearly exists, i.e. from the cutoff frequency to the maximum value of $\omega$ measured (5 MHz).

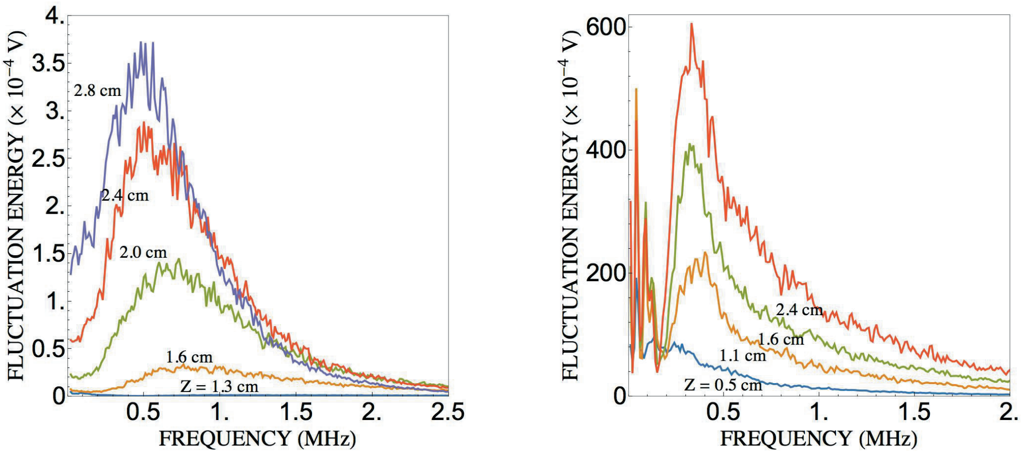


(a) (b)

Figure 5: a) Energy spectra of fluctuations in cathode plume as a function of distance from keeper for the case of $I_D = 100$ A and $\dot{m} = 10$ sccm. (b) The same parameter for the case of $I_D = 20$ A and $\dot{m} = 5$ sccm.

With this in mind, we show in Figs. 6(a) and (b) the total wave energy $E_T$ (the integral of the energy spectrum) as a function of distance from the keeper for the $\dot{m} = 5$ and 15 sccm representative cases. It is immediately evident from these plots that the total wave energy exhibits an exponential increase in amplitude. At a distance of $\sim 1.5$ cm, however, this amplitude reaches a peak and either plateaus or begins a gradual decrease. The exponential increase with position is consistent with the theoretical discussion we formulated in Sec. II.C. It suggests that the turbulence is being driven by a linear growth term. However, the wave saturation downstream of this exponential rise is not captured by our simple linear theory. This may be related to nonlinear effects in the plasma that ultimately work to limit the total wave energy. It also is possible that ion Landau damping is becoming dominant and saturating the wave. This indeed would be in keeping with our interpretation of the turbulence as a primary energy source for the ions. Uncovering the mechanism responsible for the saturation of ion acoustic turbulence is an on-going topic of discussion (c.f. Ref. 11 for a review) and is ultimately beyond the scope of this investigation. The exponential trend does suggest, however, that at least for part of the wave growth, the linear description is valid.

We plot in Fig. 7(a) the maximum values from the spatial plots of the turbulent energy, $\max\left[E_T\left(x\right)\right]$, as a function of operating conditions. We choose to focus on this parameter as it represents the maximum available energy from the IAT to be converted into ion energy per our discussion in Sec. II.B. From Fig. 7(a), we can see a clear trend with flow rate: higher energy turbulence occurs for lower flow rates. This is consistent with our interpretation outlined in Sec. II.C where we discussed the role of ion-neutral collisions—and by extension flow rate—on limiting the wave energy. On the other hand, for fixed flow rate above $\dot{m} = 8$ sccm, we can see that the wave energy exhibits a non-monotonic dependence on discharge current. Indeed, there is a minimum that appears to move to higher values of discharge current as the flow rate is increased. This minimum was noted in a previous investigation,[8] and it has particularly promising implications for ion energy mitigation. Specifically, since wave energy is assumed to drive the high energy ions, we may be able to curtail the onset of energetic ions by operating at these minima.

In support of this conclusion, we show in Fig. 7(b) the ion energy parameter $\sigma^2\left(v\right)$ that we measured with the radially oriented RPA over the same operating conditions investigated for Fig. 7(a). We calculated this term following the theory outlined in Sec. II.B. We first converted the energy distribution function measured with the RPA to a velocity space distribution $f_i\left(v\right)$ with the transformation $v = \sqrt{2\varphi/m_i}$ where $\varphi$ is the RPA bias. We then determined the standard deviation around the average kinetic velocity: $\sigma^2\left(v\right) = \int\left(v - V_i\right)^2 f_i\left(v\right)dv$. As can be seen from Fig. 7(b), the predicted spread in ion energies is on the order of $\approx 1$ eV. When combined with the plasma potentials shown in Fig. 4(b) this spread can result in ion energies well in excess of 50 V—more than sufficient to sputter the keeper. With that said, identifying the velocity spread with the ion temperature, $T_i$, suggests values that are higher than we anticipate given the cathode plume is assumed to be a typical non-equilibrium plasma with $T_i \ll T_e$. This discrepancy could reflect the

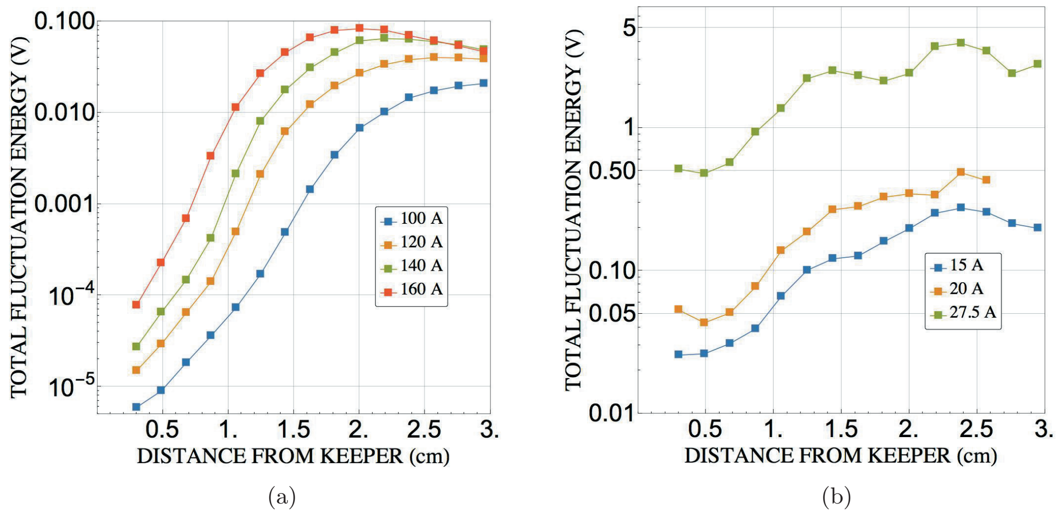


Figure 6: a) Total wave energy as a function of distance from keeper face. The flow rate is 15 sccm. (b) The same parameter but for the flow rate 5 sccm.

fact that the IAT has heated the ion velocity distribution significantly, or it is also possible that these values may be artificially broadened in part by imperfect ion optics in the RPA. Regardless of whether the ion energy variance is truly this wide or not, however, we can see that the trends depicted by the ion acoustic turbulent energy in Fig. 7(b) still are closely mirrored by the thermal spread in the ion energy distribution. The offset between the wave energy and ion energy plots—the lowest wave energy is at $10^{-3}$ V while the lowest ion energy is at $10^{-1}$ V—can be explained by the fact that the plasma, even when unheated by turbulence, has some background thermal energy. The strong correlation between the plots in Fig. 7 has the important implication that by finding the minimum in the wave energy, we can locate the discharge current where the ion energy is minimized. Moreover, if we can predict where this minimum in wave energy

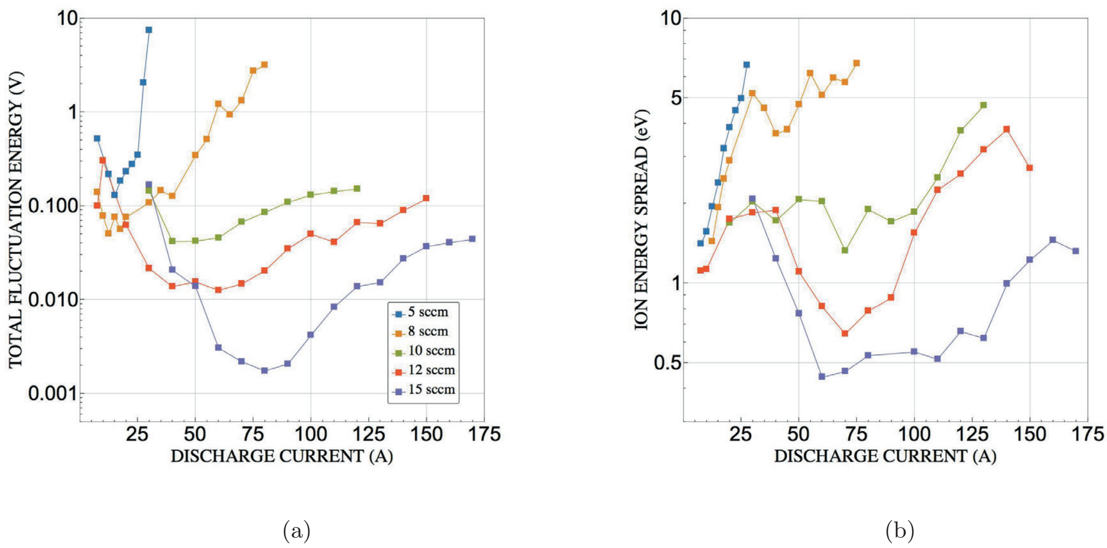


Figure 7: a) Maximum spatial wave energy as a function of discharge current for the five flow rates investigated. (b) The spread in ion energy $\sigma^2(v)$ for the same operating conditions.

will occur, we will have a means for controlling the onset of the energetic ions. The challenge is to identify how and why these minima occur. In light of the fact that turbulent energy does appear to conform to our theoretical formulation for exponential growth, it is plausible that we may be able to apply the theory we developed in Sec. II.C toward addressing this problem. We pursue this end in the following section.

### C. Comparison between theory and model

With the observation that the turbulence grows exponentially along the cathode centerline, we next turn to an assessment of our theoretical prediction for this growth. In keeping within the framework of the formulation outlined in Sec. II.C, we define a characteristic distance from the keeper where the turbulence transitions from the exponential growth to its saturated value. For the majority of the cases we examined, this occurred in the range from at 1 - 2 cm, and we thus use the value $x = 1.5$ cm in Eq. 26. As for the other parameters in this equation, we substitute the measured values reported in Sec. IV.A. The electron temperatures are provided by Fig. 4(a), and we estimate the electron drift velocity with $V_e = I_D/\left(n_e \pi r_0^2\right)$, where $r_0$ denotes the radius of the keeper orifice. For the ion collision frequency we use $\nu_{in} = V_i n_n \sigma_{in}$ where $\sigma_{in}$ is the ion-neutral cross-section ($\sim 5 \times 10^{-18}\text{cm}^{-2}$) and the neutral density is given by $n_n = \dot{m}/\left(m_i V_n \pi r_0^2\right)$. We approximate $V_{di} \approx 2,000$ m/s as is consistent with our previous experimental investigation,[10] and we make the assumption that the neutral drift velocity is thermal with temperature commensurate with the typical insert temperatures, i.e. $T = 1000$ C. Finally, we assume a cut-off frequency of $\nu_c = 2\pi/L\left(c_s + V_i\right)$ with L = 4 cm as we argued in Sec. IV.A. With these values in hand, there are two free parameters left in the model, $\beta$ and $d$, where $\beta$ is predicted to be order unity and $d \sim \mathcal{O}\left[5\right]$ mm. We have performed a parametric investigation over a range of these parameters, and the best fit yields values of $\beta = 1.1$ and $d = 4$ mm. We show the plots of this best fit next to the experimental results in Fig. 8. The constant $A' = 2.5$ was chosen to match the experimental energy levels at $\dot{m} = 15$ sccm.

The close correspondence between the model and the experimental results serves as further evidence that our quasilinear approach can be applied with success to the experimental results. Moreover, it shows that we accurately can capture the minima in the plots—suggesting that this phenomena can be explained by the interplay between the terms driving the wave growth, electron temperature and drift, and those damping the initial turbulent levels, ion-neutral collisions. Indeed, this last observation is particularly important because it provides a path forward for determining a priori where the minimum might occur. While we relied on empirically informed estimates of the driving terms—drift velocity, neutral collision frequency,

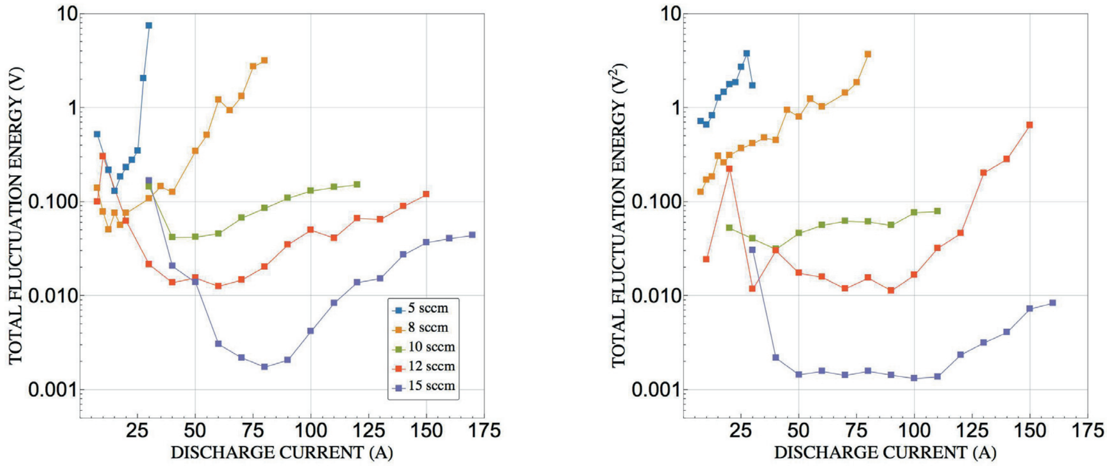


(a) (b)

Figure 8: a) Maximum spatial wave energy as a function of discharge current for the five flow rates investigated. (b) Theoretical prediction based on Eq. 26 with best fit parameters $d = 4$ mm and $\beta = 1.1$

and temperature—to evaluate Eq. 26 in this investigation, it is conceivable that we can find modeling or scaling laws that will self-consistently yield trends for the dependence of these background parameters. Such a model would allow us to move beyond the need for empirical measurements and to use a completely analytical formulation to predict the minimum in wave and ion energy.

## V. Discussion

The above results offer some guiding principles for the design of high-current hollow cathodes. At the most fundamental level, we note that in order to operate at higher current with a minimal number of energetic ions, it is necessary to increase the flow to the cathode. This conclusion has been reached empirically in the past where neutral injection was applied with success in order to mitigate the energetic ions.[20,21] However, while at first glance it would seem that the mitigation was simply the result of enhanced charge exchange collisions, an order of magnitude calculation suggests that the mean free path for this interaction in the cathode plume is several factors larger than the length scale of the plasma. The mechanism for the damping due to neutral injection thus could at best only in part be attributed to this process. On the other hand, the results from the previous sections show a very strong theoretically-predicted (Eq. 26) and experimentally-verified (Fig. 8(b)) dependence of the turbulent energy on the collision frequency. Given that the ion energy appears to be driven by the turbulence (Fig. 7), our work suggests that the damping of the acoustic turbulence at high flow rates may be responsible for the observed mitigation of energetic ions.

At a more complex level, our results go beyond the simple aphorism of higher current translating to higher flow rate. Indeed, this guiding principle naturally begs the question: how much flow and will be it effective? We have shown (Fig. 8) that for flow rates above 8 sccm there is an optimal current where turbulent energy, and therefore ion energy levels, is minimized. We further have noted through our derivation of Eq. 26 that this minimum appears to be the result of a confluence of parameters: the electron drift and temperature increase the amplitude of the turbulence while the neutral collisions damp it. Ideally, we would like to find simple scaling laws for these parameters in such a way that we could predict, before constructing a new high-current cathode, where the minimum in discharge will occur for a given flow rate and geometry. While deriving such scaling laws are beyond the scope of this investigation, there are already complex models for cathodes at low (<50 A) and high (>50 A) discharge currents[22,23] as well as some simple one-dimensional models for cathode behavior (c.f. Ref. 24) that can offer critical insight. We note, however, that these models may only have limited efficacy as they do not self-consistently include effects from the acoustic turbulence. Determining a priori the electron drift and temperature therefore may be problematic. This issue aside, the primary purpose of this investigation was to identify the most salient parameters driving the turbulence. The mitigation of the energetic ions will be achieved by using these results coupled with the appropriate scaling laws to determine the operating point where the turbulence is minimized.

## VI. Conclusion

In this investigation we have demonstrated the correlational and causal relationship between ion acoustic turbulence and energetic ions over a wide range of operating conditions for a 100-A hollow cathode. Through a one-dimensional quasilinear analysis, we have formulated an expression for the dependence of the total wave energy on plasma parameters, and we have demonstrated analytically how this total wave energy should scale with the ion energy. We have examined these theoretical results experimentally and found that not only does the turbulent energy grow exponentially along cathode centerline as predicted but that the measured ion energy is directly correlated with the maximum value the wave energy achieves during its exponential growth. We similarly have demonstrated that the turbulence amplitude (and by extension the ion energy) decreases exponentially with neutral flow rate. This explains from first principles the efficacy of previous attempts to employ supplemental neutral flow to mitigate energetic ions in hollow cathodes.[20,21]

Through a parametric study of the impact of operating conditions on wave energy, we found that at sufficiently high flow rates, this parameter exhibits a minimum with discharge current. We showed through our theoretical model that this minimum is linked to the balance between electron drift driving the turbulence and ion-neutral collisions damping it, and we demonstrated that we can estimate the location of the minimum provided we know the plasma background parameters of electron drift, ion neutral collision frequency, and temperature. As we look to the future of high-cathode currents for deep space electric propulsion, however, we ultimately would like to develop the capability for fully predictive assessments for keeper erosion. Such assessments will require models or scaling laws that self-consistently take into account the turbulent and kinetic effects outlined above. The results presented here along with the validated theoretical formulation represent the fundamental principles that will guide this effort.

In sum, the identification of what drives the turbulent energy suggests a mitigation technique for controlling high energy ions. We currently are putting this technique to the test through a shortened life study on our 100-A cathode where we have chosen the operating conditions based on the discharge current where we measured the minimum in wave energy. The result of this test, taken in conjunction with our energetic ion measurements, should serve as definitive proof for the applicability of this technique.

## Acknowledgments

The research described in this paper was carried out by the Jet Propulsion Laboratory, California Institute of Technology, under a contract with the National Aeronautics and Space Administration and funded through the internal Research and Technology Development program. The authors would like to thank Frans Ebersohn, doctoral candidate from University of Michigan, and Alex Anferov, undergraduate at the California Institute of Technology, for their assistance in data collection and analysis.

## Appendix

In order to simplify the right hand side of Eq. 13, we substitute in the diffusion operator

$$-m_i \int \left[ D_{QL} \frac{\partial f_i}{\partial v} \right] = \frac{q^2}{m_i} \sum_k \left[ k\phi_k \right]^2 \int \left( -\pi \delta \left( \omega - kv \right) + \gamma_k \frac{\partial}{\partial \omega} \mathcal{P} \left[ \frac{1}{\omega - kv} \right] \right) \frac{\partial f_i}{\partial v} dv. \tag{29}$$

We now want to express this quantity in terms of the wave energy and power density. To this end, we note from the definition of wave energy density that for a mode with wavenumber $k$, we have

$$W_k = \frac{\epsilon_0}{2} k^2 \phi^2 \omega \frac{\partial \epsilon_r}{\partial \omega_r}, \tag{30}$$

where $\omega_r$ denotes the real component of the wave frequency and $\epsilon_r$ is the real component of the dielectric tensor. For electrostatic modes, the real component of the dielectric tensor given by

$$\epsilon_r = 1 + \frac{q^2}{\epsilon_0} \sum_s \frac{1}{k m_s} \int \mathcal{P} \left[ \frac{1}{\omega - kv} \right] \frac{\partial f_s}{\partial v} dv. \tag{31}$$

For a Maxwellian plasma with ion acoustic waves characterized by $\omega / k \ll v_e$, where $v_e$ is the electron thermal velocity, we can show that the electron contribution to this equation for the dielectric tensor is independent of $\omega$. We therefore can write

$$\frac{q^2}{m_e \epsilon_0} \frac{1}{k} \int \mathcal{P} \left[ \frac{1}{\omega - kv} \right] \frac{\partial f_e}{\partial v} dv \to 0. \tag{32}$$

We thus find for the energy density that

$$W_k = \frac{q^2}{2 m_i} k \phi^2 \int \omega \frac{\partial}{\partial \omega} \mathcal{P} \left[ \frac{1}{\omega - kv} \right] \frac{\partial f_i}{\partial v} dv. \tag{33}$$

Similarly, we can show from kinetic theory (c.f Ref. 14) that

$$\gamma_k = \frac{\pi \sum_s \int \delta \left( \omega - kv \right) \frac{\partial f_s}{\partial v} dv}{\sum_s \int \frac{\partial}{\partial \omega} \mathcal{P} \left[ \frac{1}{\omega - kv} \right] \frac{\partial f_s}{\partial v} dv}. \tag{34}$$

Again invoking the result from Eq. 32, we find

$$\gamma_k = \frac{\pi \sum_s \int \delta \left( \omega - kv \right) \frac{\partial f_s}{\partial v} dv}{\int \frac{\partial}{\partial \omega} \mathcal{P} \left[ \frac{1}{\omega - kv} \right] \frac{\partial f_i}{\partial v} dv}. \tag{35}$$

The implication of this result is that

$$\gamma_{k(i)} \int \frac{\partial}{\partial \omega} \mathcal{P}\left[\frac{1}{\omega - kv}\right] \frac{\partial f_i}{\partial v} dv = \pi \int \delta\left(\omega - kv\right) \frac{\partial f_i}{\partial v} dv, \tag{36}$$

where implicitly we have use the fact that growth rate is the sum of the ion and electron contributions: $\gamma_k = \gamma_{k(i)} + \gamma_{k(e)}$. With this ion growth rate, we now can re-write Eq. 29 as

$$-m_i \int \left[D_{QL} \frac{\partial f_i}{\partial v}\right] = \frac{q^2}{m_i} \sum_k \gamma_{k(e)} \left[k\phi_k\right]^2 \int \frac{\partial}{\partial \omega} \mathcal{P}\left[\frac{1}{\omega - kv}\right] \frac{\partial f_i}{\partial v} dv. \tag{37}$$

Invoking the definition of energy density from before from Eq. 30, this result can be expressed as

$$-m_i \int \left[D_{QL} \frac{\partial f_i}{\partial v}\right] = 2 \sum_k \gamma_{k(e)} \frac{k}{\omega} W_k \tag{38}$$

Now, we know from the plasma wave kinetic equation (c.f. Ref. 14) that at steady-state, the spatial growth of the mode with wavenumber $k$ is dictated by

$$\frac{\partial \omega}{\partial k} \frac{\partial N_k}{\partial x} = 2\gamma_k N_k, \tag{39}$$

where $N_k = W_k/\omega$ is the wave action. Assuming a linear dispersion relation as is consistent with acoustic modes, we can we-write this expression as

$$\frac{\partial N_k}{\partial x} = 2\left(\gamma_{k(e)} + \gamma_{k(i)}\right) N_k \frac{k}{\omega}, \tag{40}$$

where we have broken up the growth rate into its two constituent parts. This ultimately yields

$$-2\gamma_{k(i)} N_k \frac{k}{\omega} + \frac{\partial N_k}{\partial x} = 2\gamma_{k(e)} N_k \frac{k}{\omega}. \tag{41}$$

We multiply the expression by $\omega$ in order to relate the terms to wave energy density to find

$$-2\gamma_{k(i)} W_k \frac{k}{\omega} + \frac{\partial W_k}{\partial x} = 2\gamma_{k(e)} W_k \frac{k}{\omega}. \tag{42}$$

Using this result, Eq. 38, the value of $\gamma_{k(i)}$ from Eq. 4, and the definition $P_k = \omega W_k$, we recover the expression shown in Eq. 14.

## References


[1]Polk, J., Anderson, J., Brophy, J., Rawlin, V., Patterson, M., Sovey, J., and Hamley, J., "An overview of the results from an 8200 hour wear test of the NSTAR ion thruster," *AIAA Paper, 99-2446. June, 1999*.

[2]Sengupta, A., Brophy, J. R., and Goodfellow, K. D., "Status of the extended life test of the Deep Space 1 flight spare ion engine after 30,352 hours of operation," *39th Joint Propulsion Conference, Huntsville, AL, July 20-23, 2003. AIAA-03-04558*.

[3]Brophy, J. and Garner, C., "Tests of High-Current Cathodes for Ion Engines," *24th AIAA/ASME/SAE/ASEE Joint Propulsion Conference,Boston, MA, 1988, AIAA-88-2193*.

[4]Goebel, D. M., Jameson, K. K., Katz, I., and Mikellides, I. G., "Potential fluctuations and energetic ion production in hollow cathode discharges," *Physics of Plasmas*, Vol. 14, No. 10, 2007.

[5]Mikellides, I. G., Katz, I., Goebel, D. M., Jameson, K. K., and Polk, J. E., "Wear Mechanisms in Electron Sources for Ion Propulsion, II: Discharge Hollow Cathode," *Journal of Propulsion and Power*, Vol. 24, No. 4, July 2008, pp. 866–879.

[6]Friedly, V. and Wilbur, P., "High current hollow cathode phenomena," *Journal of Propulsion and Power*, Vol. 8, No. 3, 2008, pp. 635–643.

[7]Farnell, C. C., Williams, J. D., and Farnell, C. C., "Comparison of hollow cathode discharge plasma configurations," *Plasma Sources Science and Technology*, Vol. 20, No. 2, 2011.

[8]Jorns, B. A., Mikellides, I. G., and Goebel, D. M., "Ion acoustic turbulence in a 100-A $LaB_6$ hollow cathode," *Phys. Rev. E*, Vol. 90, Dec 2014, pp. 063106.

[9]Mikellides, I. G., Katz, I., Goebel, D. M., and Jameson, K. K., "Evidence of nonclassical plasma transport in hollow cathodes for electric propulsion," *Journal of Applied Physics*, Vol. 101, No. 6, 2007, pp. 063301.

[10]Jorns, B., Goebel, D. M., and Mikellides, I. G., "Investigation of Energetic Ions in a 100-A Hollow Cathode," *50th AIAA/ASME/SAE/ASEE Joint Propulsion Conference and Exhibit, Cleveland, OH, July 28-30, 2014. AIAA-2014-3826*.

[11]Bychenkov, V., Silin, V., and Uryupin, S., "Ion-acoustic turbulence and anomalous transport," *Physics Reports*, Vol. 164, No. 3, 1988, pp. 119 – 215.

[12]Ishihara, O. and Hirose, A., "Quasilinear Mechanism of High-Energy Ion-Tail Formation in the Ion-Acousic Instability," *Physical Review Letters*, Vol. 46, No. 12, 1981.

[13]Porkolab, M. and Chang, R. P. H., "Nonlinear wave effects in laboratory plasmas: A comparison between theory and experiment," *Rev. Mod. Phys.*, Vol. 50, Oct 1978, pp. 745–795.

[14]Stix, T., *Waves in Plasmas*, AIP, New York, 1992.

[15]Williams, G.J., J., Smith, T., Domonkos, M., Gallimore, A., and Drake, R., "Laser-induced fluorescence characterization of ions emitted from hollow cathodes," *Plasma Science, IEEE Transactions on*, Vol. 28, No. 5, 2000, pp. 1664–1675.

[16]Sagdeev, R. and Galeev, A., *Nonlinear plasma theory*, Frontiers in physics, W. A. Benjamin, 1969.

[17]Chu, E. and Goebel, D. M., "High-Current Lanthanum Hexaboride Hollow Cathode for 10-to-50-kW Hall Thrusters," *Plasma Science, IEEE Transactions on*, Vol. 40, No. 9, 2012, pp. 2133–2144.

[18]Chen, F. F., "Langmuir probe diagnostics," *Mini-Course on Plasma Diagnostics, IEEE-ICOPS Meeting, Jeju, Korea*, 2003.

[19]Hutchinson, I., *Principles of Plasma Diagnostics*, Cambridge University Press, 2005.

[20]Kameyama, I., "Effects of Neutral Density on Energetic Ions Produced Near High-Current Hollow Cathodes,," Tech. Rep. NASA CR-204154, Oct. 1997.

[21]Chu, E., Goebel, D. M., and Wirz, R. E., "Reduction of Energetic Ion Production in Hollow Cathodes by External Gas Injection," *Journal of Propulsion and Power*, Vol. 29, No. 5, 2013, pp. 1155–1163.

[22]Mikellides, I. G., Katz, I., Goebel, D. M., and Polk, J. E., "Hollow cathode theory and experiment. II. A two-dimensional theoretical model of the emitter region," *Journal of Applied Physics*, Vol. 98, No. 11, 2005.

[23]Mikellides, I. G., Goebel, D. M., Jorns, B. A., Polk, J. E., and Guerrero, P., "Numerical Simulations of the Partially-ionized Gas in a 100-A LaB6 Hollow Cathode," *IEEE Transactions on Plasma Science, Special Issue on Plasma Propulsion*, Vol. 43, No. 1, 2015.

[24]Goebel, D. and Katz, I., *Fundamentals of Electric Propulsion: Ion and Hall Thrusters*, JPL Space Science and Technology Series, Wiley, 2008.